Hindawi
Structural Control and Health Monitoring
Volume 2023, Article ID 8325686, 25 pages
https://doi.org/10.1155/2023/8325686

Research Article

Structural Damage Identification considering Uncertainties in Nonuniform Measurement Conditions Based on Convolution Neural Networks

Siyu Zhu[1] **and Tianyu Xiang**[2]

[1]*College of Environment and Civil Engineering, Chengdu University of Technology, Chengdu 610059, Sichuan, China*
[2]*Department of Civil Engineering, Xihua University, Chengdu 610059, Sichuan, China*

Correspondence should be addressed to Siyu Zhu; blueskyzsy@aliyun.com

Received 7 November 2022; Revised 10 April 2023; Accepted 12 April 2023; Published 8 August 2023

Academic Editor: Chia-Ming Chang

Dynamic-vibration-based structural damage identification (SDI) represents the main target for structural health monitoring (SHM). It is significant to consider the unavoidable uncertainties arising from both the structure and measuring noise. On the other hand, nonuniform measurement conditions often appear in actual SHM applications, which consist of two parts, i.e., spatial nonuniform characteristics for noises are induced by various intensities of input noise in every single sampling channel and multisensor stays in a damaged state. This paper proposes a new method for the SDI considering uncertainties in nonuniform measurement conditions integrating convolutional neural network (CNN). Herein, the great ability of feature extraction from the measurement associated with the convolutional network is used to handle the input data, and the mapping connection between the selected features and damage states is established. Time histories of structural responses, such as acceleration, are applied for damage identification. The application and accuracy of the CNN, which is trained with input uncertain parameters contaminated by stochastic noises, are verified by the finite element numerical and experimental results. Both uncertain parameters and measurement conditions are considered in the verification. The responses obtained from the numerical and experimental approach show that the proposed neural network model can identify the structural damage with high accuracy. The great robustness of the proposed method is examined by studying the influence of uncertainties, even considering the nonuniform measurement condition.

1. Introduction

Structural damage identification (SDI), as the most important issue for the structural health monitoring system, has attracted extensive attention in civil engineering projects. Identifying damage is significant and adopted in the evaluation of the structural operating conditions and ensuring its safety, especially for important infrastructure. Various SDI methods using changes in dynamic analysis have been improved in the past decades. Doebling et al. provide a summary review of SDI techniques and applications before 1998 [1]. However, most traditional identification approaches are based on some modal information (i.e., frequency, modal shape, and curvature). Since the numbers and measuring accuracy of monitoring points are limited, the complete modal parameters before damage are difficult to conduct for the SDI systems. More measuring points should be settled, and a more significant requirement for modal experiment also needs to be obtained in practical engineering, which rapidly reduces the economic cost.

The novel studies of the SDI, from 2010 to 2019, are also summarized by Hou and Xia [2]. With the essential improvement of artificial intelligence, the machine learning on the SDI has been widely used [3, 4]. Based on the principle of the machine learning method, SDI can be assumed as the sample acknowledgment situation. Training data is always conducted from laboratory testing and structural finite element simulations. Secondly, statistical or signal processing

approaches are applied to deal with the tested responses for feature extraction. Finally, through the chosen feature, the presence, position, and severity of the structural damage can be identified based on the classification algorithm. Compared with the traditional network architecture, deep learning algorithms can automatically capture more significant information from the input training samples by using numerous hidden layers. Convolutional neural network (CNN) is one of the state-of-the-art deep neural networks, which has been widely employed for SDI using vibration responses [5]. Abdeljaber et al. proposed 1D CNNs to establish a significant structural damage detection system, which can automatically extract damage features from vibration signals and input to locate damage in real-time [6]. Duan et al. presented an automated damage identification method based on a CNN. The raw measurement accelerations are transformed into Fourier amplitude spectra for the training data of the neural network [7]. Bao et al. combined the application of computer vision with a deep learning-based data anomaly detection method, which was applied to an actual cable-stayed bridge for the verification of the proposed method [8]. Wang et al. adopted a densely connected layer to optimize the CNN for SDI, which takes the advantage of a limited number of sensors to extract the damage feature for the SDI [9]. Xu considered the multilevel and multiscale features of the input information, and a fusion CNN was proposed to deal with crack identification in bridge engineering projects [10]. Seventekidis et al. established an optimal finite element (FE) model to generate the training data for the deep learning CNN, which is verified by the experimental data on the benchmark structure [11]. Li et al. proposed a new method combining the inverse finite element method and CNN, and the strain mode differences are considered. Its localization ability and damage quantification prediction accuracy are verified [12]. Zhang et al. listed a hybrid method that connected phase-based motion estimation with CNNs to address the situation that training data for CNN is difficult to obtain in actual engineering projects [13]. Ai et al. proposed a 2D CNN integrated with electromechanical admittance, which was applied to identify compressive stress and external excitation-induced damage, and the accuracy and efficiency of the method were proved [14].

Since the quantity of modal information adopted is always larger than the actual number of elements, the SDI is regarded as a determined problem in most of the aforementioned studies. However, it is impossible to conduct enough input modal data for the SDI with the limitation of monitoring sensors or external environmental influences. In addition, uncertainties inevitably arise from either the structure or measurement [15–17], which will undermine the accuracy of SDI [15]. In addition, the damage identification of uncertain structures will cost too much in the experimental tests. Therefore, the effect of uncertainties on the SDI is always investigated based on the finite element (FE) model analysis, which includes uncertain structural parameters and modeling errors [18]. During the numerical modeling process for the structures, the input structural parameters present the random characteristics of every structure in nature. And no matter how complex and comprehensive the FE model is, it still has some unavoidable differences from the actual structure. Based on the short review of the stochastic modeling of uncertainties in computational structural dynamics [19], variations can be simulated and input into the structural parameters to study the coupling effects of several uncertainties. Pathirage et al. proposed an autoencoder-based architecture for SDI. It can use deep neural networks and be applied to learn a mapping between the dynamic characteristics and damage situations [20]. Villani et al. applied the discrete-time Volterra series expanded with Kautz filters to study the responses of a beam in an experimental test, and the uncertainties of the structure were involved. Based on the random index and hypothesis test, the method of damage detection is applied to consider the simulated damage and the loss of mass [21, 22]. Ding et al. proposed a new approach of SDI, which was based on the clustering-based tree seed algorithm and considered the FE modal errors and measuring noise. The accuracy of the proposed approach was verified by comparing it with the results from the numerical and experimental testing [23]. Fan et al. proposed a vibration signal denoising method for structural health monitoring based on residual CNN [24]. Shi et al. deduced the matrix between strain mode and the structure's element stiffness parameter, and the connection between modal information and damage coefficients of structures was established. Its applicability was proved, and its efficiency and robustness were also studied [25]. Silva et al. investigated the negative influence caused by modeling uncertainties on SDI and proposed a method for damage identification under uncertain conditions. The results estimated by approximate marginalization under uncertainties were feasible, but those by standard maximum were not [26, 27].

Recent achievements [20, 28, 29] utilized modal information to identify structural damage. Numerous sensors should be settled to cover all the structural messages, which are to conduct modal information. However, it is not realistic in data acquisition for the large-scale structure. Therefore, the time-domain SDI methods are applied to measure acceleration responses by certain sensors, which is significant that much fewer sensors are required to provide the whole dynamic information for establishing the identification equation and sample the sufficient data points. Zhang et al. have utilized the raw acceleration responses to identify the structural damage, directly [30]. Although the measured time-domain responses include the unavoidable and essential effect of noise, the deep learning methods can solve this situation because of their powerful ability to scale large data and extract underlying feature distributions [31]. However, most operating sensors are suffering damage from extreme weather, equipment technical problems, measuring environmental noise, and other factors, so the data collected by the sensors become faulty. The most common of all types of data abnormity is data loss [32]. Loss of data will result in the abandonment of significant measuring information and a serious reduction in SDI accuracy. Additionally, many deep learning-based algorithms for structural monitoring information require a sufficient training dataset to establish

the analysis framework, while data loss will cause the collapse of the calculation. Fan et al. applied a CNN with bottleneck framework and connection, which included the relationship between data loss and the complete information [33] and also presented a dynamic response reconstruction method for structural health monitoring using densely connected convolutional networks [34]. Li et al. exhibited the connection between the whole true signals and the realistic hypotheses for the lost signals [35]. If the SDI is in multisensor damaged condition, the collected signals become meaningless noises and present strong nonuniform characteristics in measuring accuracy of sensors. Therefore, the situation of the losing data for the sensors can be regarded as the extremely issue of SDI. Therefore, it is worthwhile to study the effect of the nonuniform measuring conditions on the SDI by the CNN.

In this paper, a new deep learning neural network framework for SDI with uncertain parameters is proposed. And the time-domain acceleration responses of structure, which are conducted by both the finite element analysis and experimental testing, are explored to extract the damage-related samples for SDI. In addition, since the signals captured by random sensors include the stochastic noises, the nonuniform characteristics in measurement condition are involved and their effects on the identification by CNN are studied. The extreme issue for the nonuniform measurement condition, namely, the multisensor damaged state, is also considered.

2. Methodologies

CNNs have a significantly powerful capability for feature extraction. The intact and damaged states of the target structure are regarded as the training information for the CNNs. The distribution information of the intact and damaged states of the structure can be learned, and the features of the intact and damaged structure can be extracted. If a new structure is an input into the established CNN model, it can immediately make judgments and identify whether the structure is damaged so as to achieve the target of SDI. The relationship of signals obtained by a series of sensors can be simulated as the modal information of the target structure, which can be applied to identify the damaged state based on CNNs. In this paper, the structural dynamic accelerations are used to establish a two-dimensional matrix which can reflect the structural modal shape. This matrix and the corresponding labels are severed as input training data for the CNNs and get through convolution and pooling layers, and the local receptive field can realize the feature extraction of acceleration responses. Finally, moving through the full connection layers, the mapping relationship between input dynamic responses and the structurally damaged state is established, as shown in Figure 1, which presents strong distinguishing ability and generalization performance.

The CNN model for SDI can be divided into two parts: the training and prediction networks, as shown in Figure 2. The training network deals with learning the feature from the structural modal and damaged information and capturing the weight and threshold value. In addition, the conducted acceleration responses are used as input information for the prediction network, and the structural damage probability can be carried out based on the weight and threshold value, so as to identify whether the structure is damaged or not.

Therefore, the framework of the CNN model, which is used to identify the structural damage, is proposed and shown in Figure 3. It consists of 12 layers, including 1 input layer, 3 convolution layers, 3 pooling layers, 3 full connection layers, 1 Softmax layer, and 1 output layer. The parameters of the CNNs framework are listed in Table 1.

(1) The first layer is the input layer, and the size of the input samples is based on the corresponding input data. A matrix, which can be written as 1 @, is taken as an example to explain the working process of CNN framework. n represents the number of sensors, and m is the sampling number in every sensor.

(2) The 2nd, 4th, and 6th layers, respectively, are convolution layers, marked as C1, C2, and C3, and the same convolution operation mode is suitable for them. The number of convolution kernels is c_1, c_2, and c_3, and the size of every convolution kernel is $a_1 \times a_1$, $a_2 \times a_2$, and $a_3 \times a_3$, and the sliding step is s_c. The ReLU function is applied as the activation function.

(3) The 3rd, 5th, and 7th layers are pooling layers, marked as P1, P2, and P3, and the maximum pooling method is adopted. The number of pooling bins is p_1, p_2, and p_3, and their sizes are $b_1 \times b_1$, $b_2 \times b_2$, and $b_3 \times b_3$, and the sliding step is s_p. After going through 3 convolution and 3 pooling layers, the original matrix 1 @ is extracted as c_3 @ ceil (ceil (ceil $(n/b_1)/b_2)/b_3) \times$ ceil (ceil (ceil$(m/b_1)/b_2)/b_3$), which is recorded as the t_0 vector. ceil$(\cdot)$ represents ceil rounding function.

(4) The 8th, 9th, and 10th layers are full connected layers, denoted as F1, F2, and F3, which apply the sigmoid activation function. The full connected layer F1 "flattens" the convolutional pooled t_0 vector into a vector $1@1 \times (\text{ceil}(\text{ceil}(\text{ceil}(m/b_1)/b_2)/b_3) \cdot c_3)$, and the "flattened" vector is denoted as t_1 vector. The "flattened" t_1 vector is transmitted and compressed through the F2 and F3, and the t_2 and t_3 vector, respectively, is obtained in F2 and F3.

(5) The 11th layer is also the full connection layer, but the Softmax function is severed as the highest layer of the network and called the Softmax layer. The compressed t_3 vector in F3 is classified into two categories, "0" and "1."

(6) The 12th layer is the output layer. When the output is "1," it means the structure stays in a good operational situation. On the contract, the structure is damaged if the output is "0."

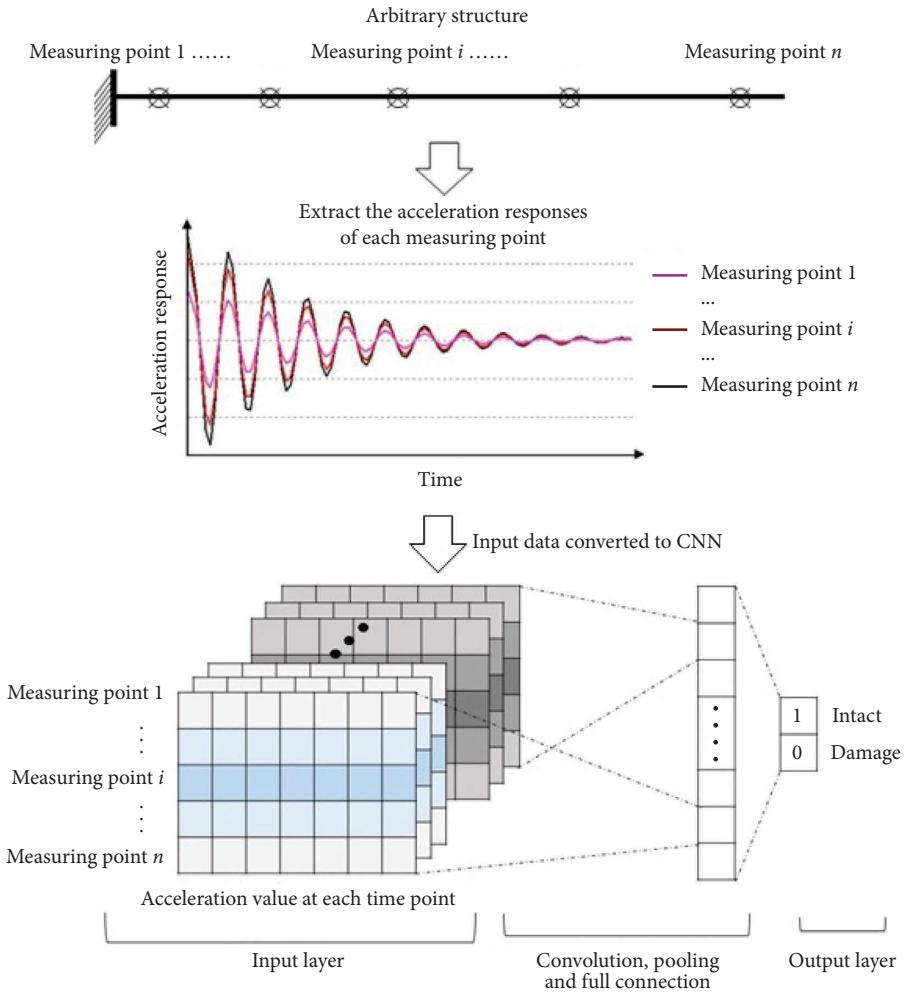

Figure 1: The principle of CNN in SDI.

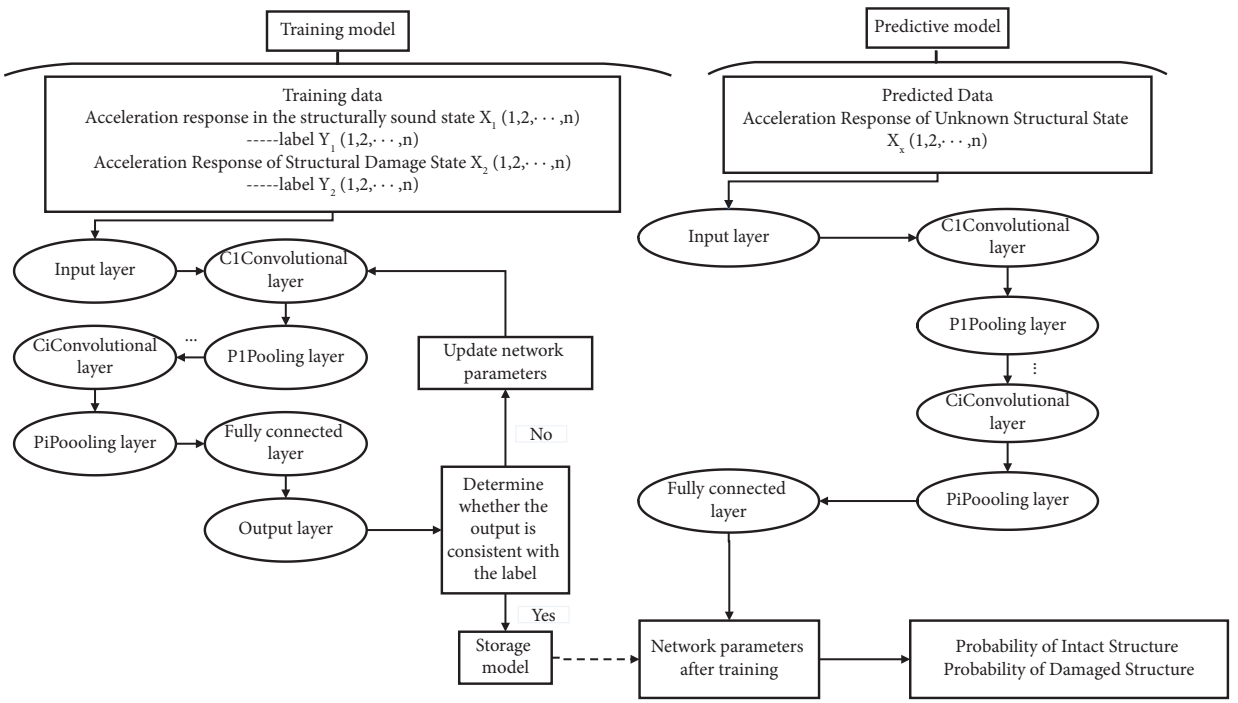

Figure 2: CNN model for SDI.

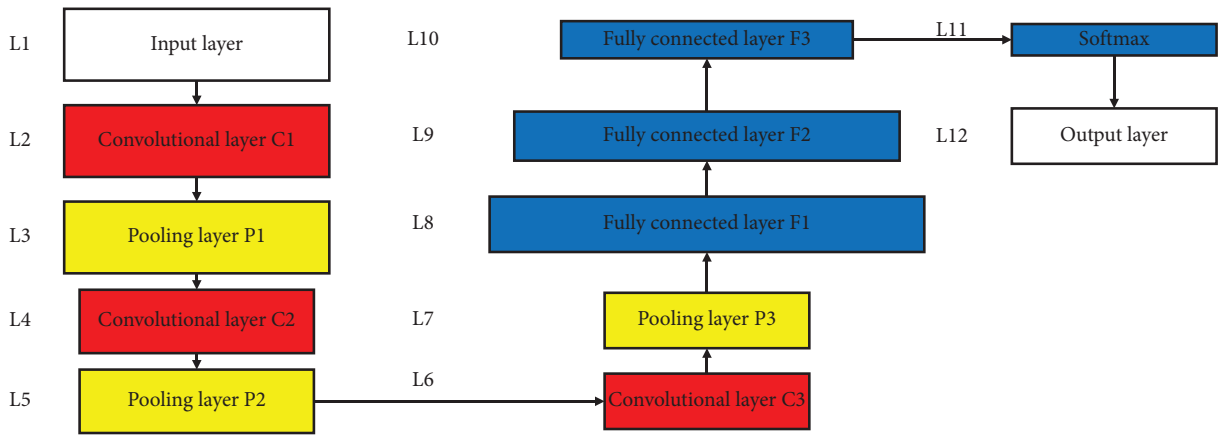

Figure 3: The framework of CNN model.

In the table,

$$
\begin{aligned}
\overrightarrow{O_3} &= c_1@\mathrm{ceil}\left(\frac{n}{b_1}\right)\times\left(\mathrm{ceil}\left(\frac{m}{b_1}\right)\right),\\
\overrightarrow{O_4} &= c_2@\mathrm{ceil}\left(\frac{n}{b_1}\right)\times\left(\mathrm{ceil}\left(\frac{m}{b_1}\right)\right),\\
\overrightarrow{O_5} &= c_2@\mathrm{ceil}\left(\frac{\mathrm{ceil}\left(n/b_1\right)}{b_2}\right)\times\mathrm{ceil}\left(\frac{\mathrm{ceil}\left(m/b_1\right)}{b_2}\right),\\
\overrightarrow{O_6} &= c_3@\mathrm{ceil}\left(\frac{\mathrm{ceil}\left(n/b_1\right)}{b_2}\right)\times\mathrm{ceil}\left(\frac{\mathrm{ceil}\left(m/b_1\right)}{b_2}\right),\\
t_0 &= c_3@\mathrm{ceil}\left(\frac{\mathrm{ceil}\left(\mathrm{ceil}\left(n/b_1\right)/b_2\right)}{b_3}\right)\times\mathrm{ceil}\left(\frac{\mathrm{ceil}\left(\mathrm{ceil}\left(m/b_1\right)/b_2\right)}{b_3}\right),\\
t_1 &= 1@1\times z,\\
z &= \left(\mathrm{ceil}\left(\frac{\mathrm{ceil}\left(\mathrm{ceil}\left(m/b_1\right)/b_2\right)}{b_3}\right)\cdot c_3\right),\\
t_2 &= 1@1\times u,\\
t_3 &= 1@1\times v,u,v,
\end{aligned}
\tag{1}
$$

which are positive integers that are less than z or bigger than 2.

3. Verification of the SDI Based on CNNs

3.1. SDI of Finite Element Model. A simply supported bridge for the testing experiment is applied, and the settlement of sensors is shown in Figure 4, which is taken to verify the application of the CNNs to identify the structural damaged condition. Firstly, the finite element model is established according to the selected structure, and the acceleration responses of the structure are obtained through numerical simulation. Secondly, they are used as the input data, and the CNN model is obtained based on the acceleration responses, which are used as training data for CNNs. Finally, the accuracy of CNN is verified by the experimental testing.

As shown in Figure 5, the I-beam is applied for the simply supported bridge. The full length of each main beam is 2.2 m, the calculated span is 2.1 m, and the center spacing of the main beam is 0.2 m. Steel batten plates are used as the transverse connection, which has a size of 0.15 m × × 0.22 m × 0.05 m.

Table 1: Parameters of CNN model.

Network layer	Module	Input	Computing cores	Computing cores	Sliding step	Output points
L1	Input layer	$1 @ n \times m$	—	—	—	$1 @ n \times m$
L2	Convolutional layer C1	$1 @ n \times m$	c_1	$a_1 \times a_1$	s_c	$c_1 @ n \times m$
L3	Pooling layer P1	$c_1 @ n \times m$	p_1	$b_1 \times b_1$	s_p	$\overrightarrow{O_3}$
L4	Convolutional layer C2	$\overrightarrow{O_3}$	c_2	$a_2 \times a_2$	s_c	$\overrightarrow{O_4}$
L5	Pooling layer P2	$\overrightarrow{O_4}$	p_2	$b_2 \times b_2$	s_p	$\overrightarrow{O_5}$
L6	Convolutional layer C3	$\overrightarrow{O_5}$	c_3	$a_3 \times a_3$	s_c	$\overrightarrow{O_6}$
L7	Pooling layer P3	$\overrightarrow{O_6}$	p_3	$b_3 \times b_3$	s_p	t_0
L8	Fully connected layer F1	t_0	—	—	—	t_1
L9	Fully connected layer F2	t_1	—	—	—	t_2
L10	Fully connected layer F3	t_2	—	—	—	t_3
L11	Softmax layer	t_3	—	—	—	$1@1 \times 2$
L12	Output layer	$1@1 \times 2$	—	—	—	The probability of two categories of “0” and “1”

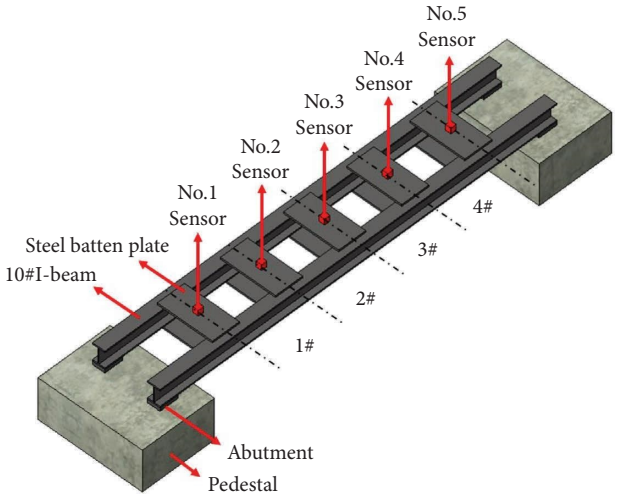

Figure 4: Settlement of the sensors of the experimental structure.

The center spacing between adjacent batten plates is 0.35 m, and the net distance is 0.2 m.

The finite element model is established by ANSYS software. To make the finite element model closer to the test structure, Shell 63 element is used for modeling and is shown in Figure 6. The parameters of the finite element are shown in Table 2.

For the finite element model, the total length of the structure is 2.1 m which is divided into 24 segments, and each segment is composed of 5 plate elements. The center distance between the two main beams is 0.2 m, and they are connected by batten plates. The simulation of battens consists of four plate elements. There are 370 nodes and 280 plate elements in the whole model, and the total mass of the structure is 71.60 kg, of which the mass of the main beam is 47.58 kg. According to the actual structural damage location, the elements at the corresponding damaged position should be deleted, which is applied to simulate the damaged condition for the FE model. The method of simulating structural damage in the finite element model is to directly delete the element corresponding to the actual structural damage location. In addition, the pulse excitation input is adopted as the external load for the SDI in the FE model, which vertically affects the random position of the top of the main beams. During the loading process of the simulation, the initial effect time is randomly selected from the range 0.0~1.2 s. Therefore, there are 5 channels, which are the same as 5 sensors at the experimental testing, to capture dynamic acceleration responses, as shown in Figure 6. The sampling frequency of each channel is 200 Hz, which means the capturing time of 300 data points is 1.5 s. Therefore, the size of every sample in CNNs is 5×300. Figure 7 shows the structural acceleration responses of the FE model under certain pulse excitation.

3.2. SDI Based on Experimental Testing. The experimental model for the testing is shown in Figure 8, which is similar to the FE model. The monitoring point is settled at the center of the top of the batten plate, and the acceleration sensor and the structure are bonded with grease, which ensures that there is no relative displacement between them.

There are 4 sections for the testing structure, named 1#~4#, as shown in Figure 4. The structural damage condition in the test is achieved by cutting the outer lower flanges of each segment of the two main beams. Therefore, 4 damaged working conditions are considered, as shown in Table 3, in which the midpoint of the cutting block is the center of every segment, the length of the block is 17 cm, and the width is 2 cm, as shown in Figure 9.

The pulse excitation is effected on the testing structure, as shown in Figure 10. The details of the external loads are listed in Table 4. 5 sensors were used in the testing, and the sampling frequency was 200 Hz. Figure 11 shows the acceleration responses of the structure under certain pulse excitation. According to the principle of CNN for SDI and the size of the training sample in this experiment, the framework and parameters of the CNN model are designed as shown in Table 5.

4000 groups of acceleration calculated by the FE model are applied as the training data for the CNN model, including 2000 groups for no-damaged structures and others for damaged ones. The size of every group of acceleration is $5 \times \times 300$. In addition, there are 2000 groups of acceleration obtained from the FE model and experimental testing, respectively, which are involving no-damaged and damaged structure and adopted as the prediction samples for the CNN. The prediction samples include 2000 groups of no-damaged structural responses and 2000 groups of damaged ones, which is a randomization. The ratio of the number of groups of identified results by CNN to the number of groups of prediction samples is defined as the identified accuracy of the CNN for SDI, also named the identified ratio (IR). The IR obtained by comparing CNN with the FE model or the experimental testing is listed in Figures 12 and 13. For the FE model, the minimum IR of CNN is 84.6%, and the maximum of that is 93.8% among all the four cases. In addition, the range of IR of CNN with the experimental testing is from 81.9% to 90.1%. Therefore, the identified accuracy of CNN for SDI satisfies the computational requirement, and CNN is a reliable tool for structural damage detection.

4. Effect of Structural Uncertainties on SDI Based on CNN

The acceleration responses conducted by numerical simulation are regarded as the input training data for CNN when the CNN is applied to identify the structural damage situation. The CNN is trained by the deterministic structural responses; however, the uncertainties arising from the structure are unavoidable, and the structural damage condition will make the matrix of stiffness, mass, and damping ratio change. Therefore, it is significant to investigate the effect of the uncertain parameters on the accuracy of the SDI based on CNN. The cross-section of the simply supported bridge is rectangular with a height of 0.3 m and a width of 0.2 m. The span of the bridge is 2.0 m, and the whole beam is divided into 20 elements, which is shown in Figure 6. The mass density of the structure is 2500 kg/m^3, the elastic

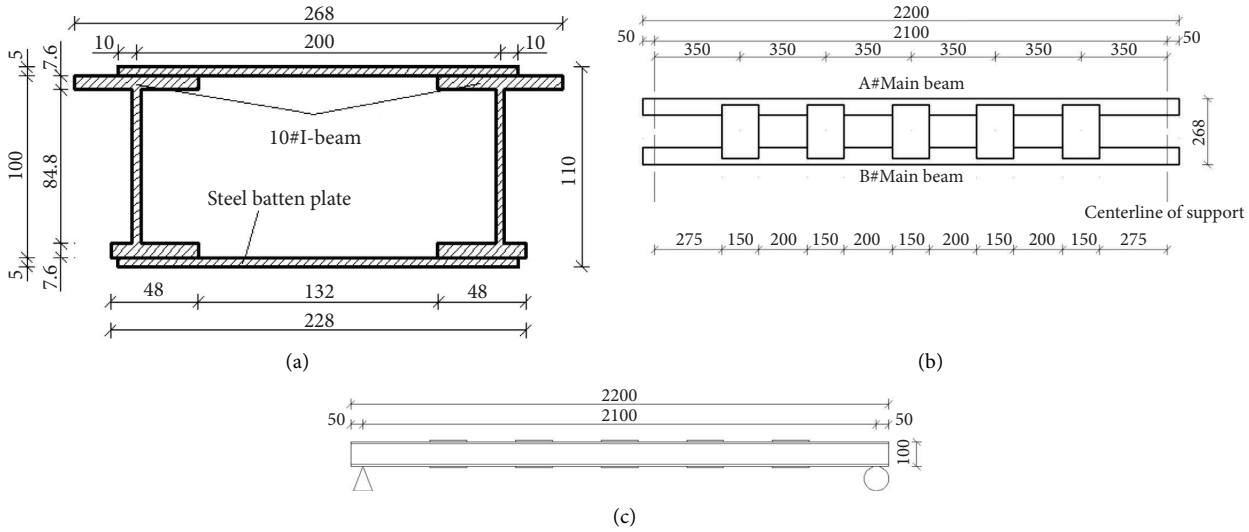

Figure 5: Detailed dimensions of the test structure (unit: mm). (a) Structural cross-section size. (b) Structural plane size. (c) Structural facade size.

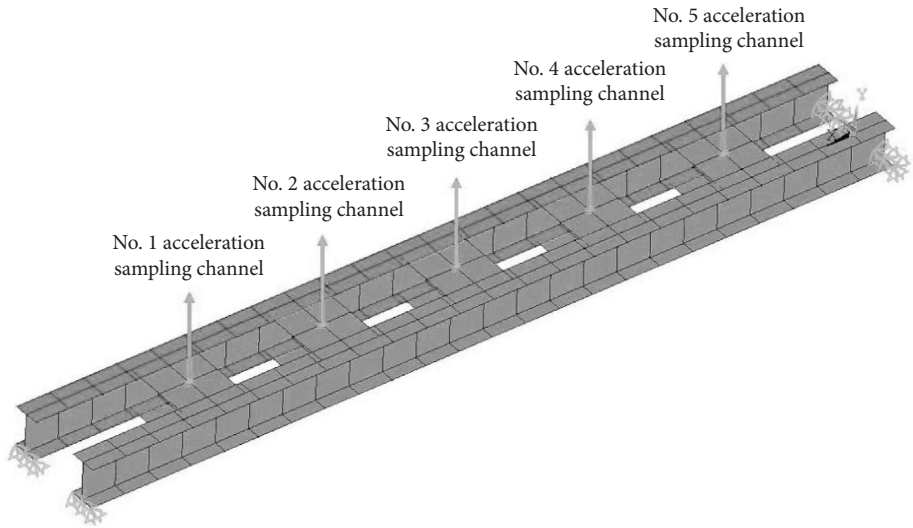

Figure 6: Finite element model of the test structure.

Table 2: Model parameter.

Parameter type	Parameter name	Take value
Parameters of section properties	Thickness of I-beam roof plate	7.6 mm
	Thickness of I-beam bottom plate	7.6 mm
	Thickness of I-beam web	4.5 mm
	Thickness of batten plate	5.0 mm
Parameters of material properties	Mass density	8006 kg/m^3
	Elastic modulus	2.06 $\times 10^5$ MPa
	Poisson's ratio	0.31
	Damping ratio	0.01
Parameters of structure properties	Length of main beam	2.1 m
	Total number of nodes	370个
	Total number of elements	280个
	Boundary constraints	Simply supported beam constraint

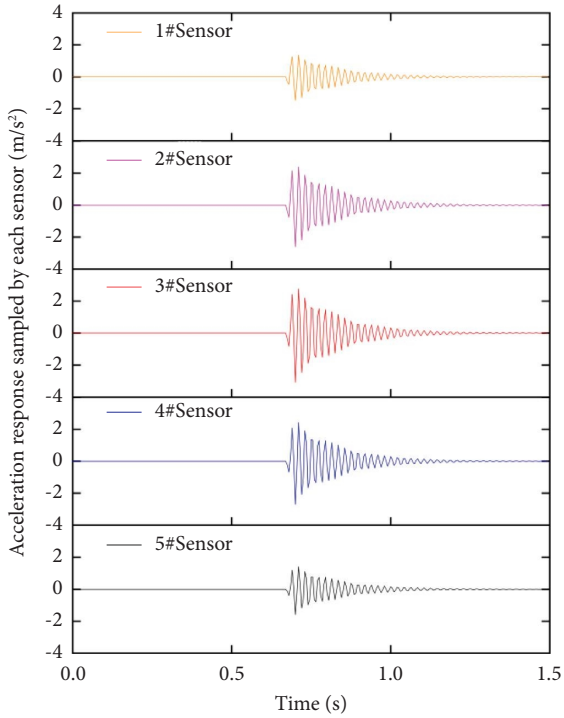

Figure 7: Finite element data of the test.

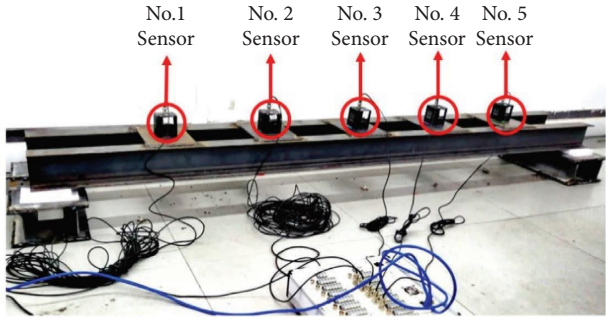

Figure 8: Actual model of the test structure.

Table 3: Case of the test.

Numbering	Description of the case of the test
Damage case 1	Damage 2# sections outer lower flange
Damage case 2	Damage 2# and 3# sections outer lower flange
Damage case 3	Damage2#, 3#, and 4# sections outer lower flange
Damage case 4	Damage1#, 2#, 3#, and 4# sections outer lower flange

modulus $E = 3.0 \times \times 10^4$ MPa, the moment of inertia $I = 4.5 \times \times 10^{-4}$ m^4, and the damping ratio is 0.02. The damage issue can be expressed as the stiffness reduction of the structure. Therefore, the decreasing material stiffness EI is used to simulate the damage issue, in which the original stiffness EI of every element multiplies with a reducing coefficient α_i. The new stiffness is shown as $\alpha_i \cdot EI$, and the reducing coefficient α_i is selected from random numbers that follow a uniform distribution in the range of 0.3~1.0. The external excitation is also severed as the pulse excitation, and its details are listed in Table 6. Taking 5 nodes (No. 4, 7, 11, 15, and 18) as the target points to list their acceleration responses, whose sampling frequency is 1000 Hz. Every point should capture 100 series of acceleration responses. Therefore, a size of 5×100 matrix, shown in Figure 14, can be simulated based on the conducted acceleration responses, which is similar to the size of a 5×100 photo and is adopted as training data for CNN.

The uncertain parameters of structure, such as mass, elastic modulus, and damping ratio, are considered in the SDI based on CNN, which follows a normal distribution. The mean value and coefficient of variation (COV) of the involved parameters are shown in Table 7. Four cases are selected to investigate the application of CNN on uncertain SDI, and they are exhibited in Table 8.

As shown in the table, the effect of single one parameter on the IR by CNN is studied in Case 1~3, and corresponding time histories of acceleration are shown in Figures 15–17. In addition, the coupling effect of three parameters is also calculated, and the results of Case 4 are shown in Figure 18.

The parameters of the CNN for SDI are listed in Table 9. For the aforementioned cases with uncertainties, 4000 groups of acceleration with the size of 5×100 matrix are adopted as the training sample sets, including no-damaged and damaged conditions. And the number of the prediction for CNN is also 4000 with two structural conditions (no-damaged and damaged). The sampling noises are ignored. The datasets from simulation are selected randomly as the training data, and those from experiment are chosen as the prediction data. The IR is applied to evaluate the identified accuracy of structural damage by CNN, which is shown in Figure 19. As shown in the figure, the uncertain damping ratio has little influence on the IR of the structural damage by the CNN, the IRs are bigger than 99.4% with different COVs of damping ratio. For the other three cases, the IRs are decreasing with the development of COV of the involved uncertainties. The effect of the uncertain mass is equal to that of elastic modulus. The IR in Case 1 is 81.13% and that in Case 2 is 81.55%, when the COV of the corresponding random variable is 0.30. In addition, the IR in Case 4 presents a more rapid reduction than in Case 1 and 2, which means the effect of the coupling of three parameters is enhanced and further reduces the IR. The IR of structural damage by CNN is smaller than 80%, which cannot satisfy the requirements of the SDI based on CNN in Case 4. Therefore, based on the training data without uncertainties, the established CNN framework cannot guarantee the identified accuracy of the structural damage when several structural uncertainties are considered in prediction and the corresponding COVs are large.

In addition, to further investigate the effect of uncertainties on the identified accuracy of structural damage by CNN, a new CNN framework is proposed whose training data need to consider the effect of uncertain parameters. In this part, the original CNN is named CNN 1 based on the training data without uncertainties, and the new CNN is named CNN 2 based on that with three uncertainties. The

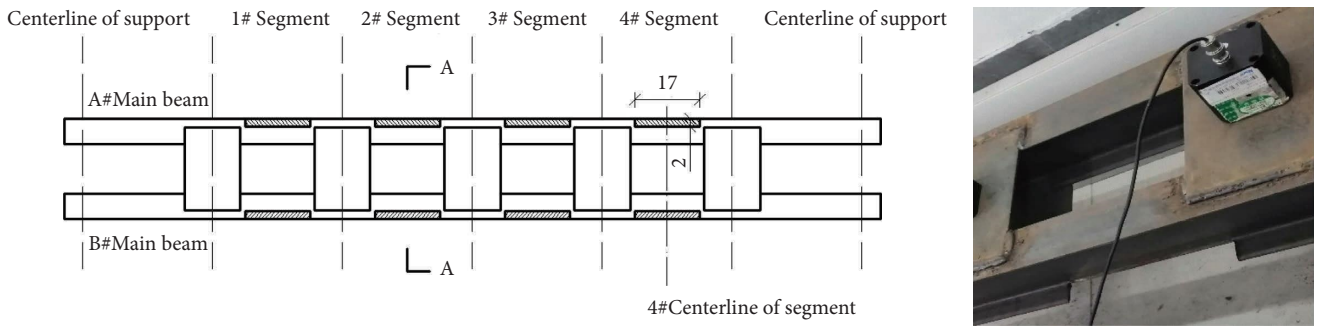

Figure 9: Test structure after damage. (a) Plane (unit: mm). (b) Actual damage.

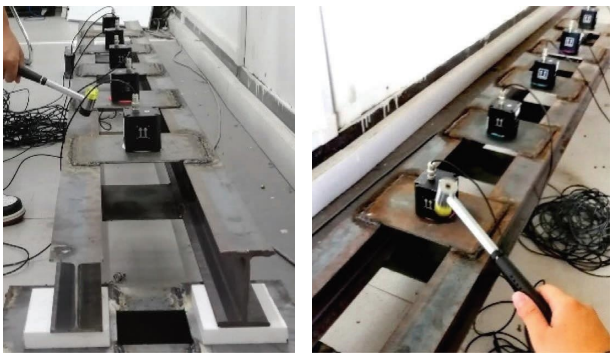

Figure 10: Test structure subjected to pulse excitation.

Table 4: Parameters of pulse excitation.

Category	Range of taking values
Direction of pulse excitation	Vertical down
Pulse excitation point of action	The two main beam roofs without support
The time point of pulse excitation	Any random number in 0 s~1.2 s

prediction results involve all the uncertainties for two types of CNN framework. The sampling noises are also ignored. The IR of the two types of CNN models is presented in Table 10. As a result, without input signal noises, the uncertainties involved in training data have few effects on the identified accuracy of structural damage.

However, the measuring noises are unavoidable during the process of capturing acceleration responses by sensors. Therefore, to further reflect the authenticity of the CNN to identify the actual structural damage situation, the original acceleration signals should add the measuring noise, which is based on the principle of signal noise ratio (SNR) [36]. The mean value of noise reflects the intensity of noise, the intensity of noise is expressed by the signal-to-noise ratio, and the variance of noise reflects the nonuniform characteristics of noise. The definition of the signal-to-noise ratio is shown as follows:

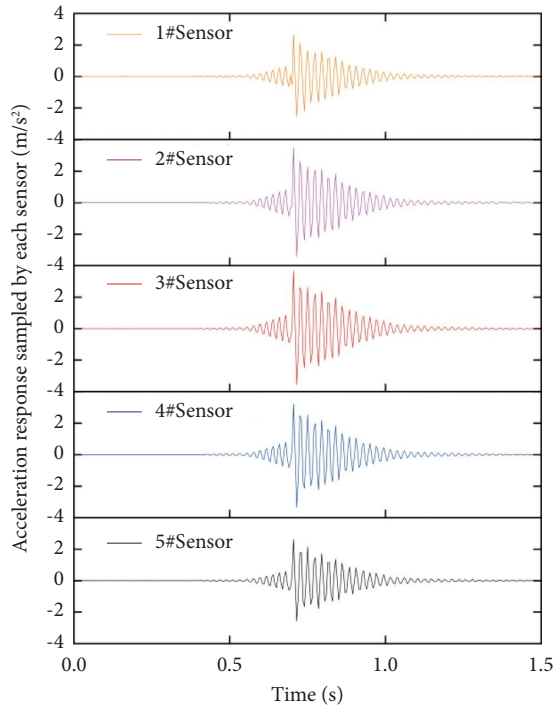

Figure 11: Measured data of the test.

Table 5: Parameters of the CNN model.

Network layer	Module	Input (number@ number of channels × number of channel sampling points)	Number of computing cores	Size of computing cores	Sliding step	Output (number@ number of channels × number of channel sampling points)
L1	Input layer	1@5 × 300	—	—	—	1@5 × 300
L2	Convolutional layer C1	1@5 × 300	10	5 × 5	1	10@5 × 300
L3	Pooling layer P1	10@5 × 300	1	2 × 2	2	10@3 × 150
L4	Convolutional layer C2	10@3 × 150	10	5 × 5	1	10@3 × 150
L5	Pooling layer P2	10@3 × 150	1	2 × 2	2	10@2 × 75
L6	Convolutional layer C3	10@2 × 75	10	5 × 5	1	10@2 × 75
L7	Pooling layer P3	10@2 × 75	1	2 × 2	2	10@1 × 38
L8	Fully connected layer F1	10@1 × 38	—	—	—	1@1 × 380
L9	Fully connected layer F2	1@1 × 380	—	—	—	1@1 × 150
L10	Fully connected layer F3	1@1 × 150	—	—	—	1@1 × 40
L11	Softmax layer	1@1 × 40	—	—	—	1@1 × 2
L12	Output layer	1@1 × 2	—	—	—	The probability of two categories of “0” and “1”

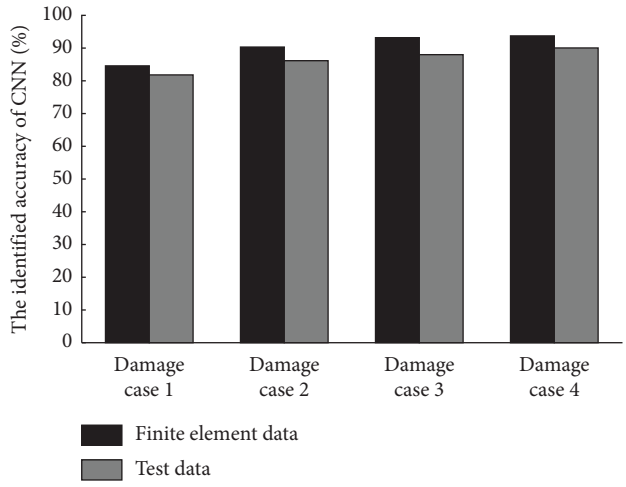

Figure 12: Identification accuracy of CNN model for the verification.

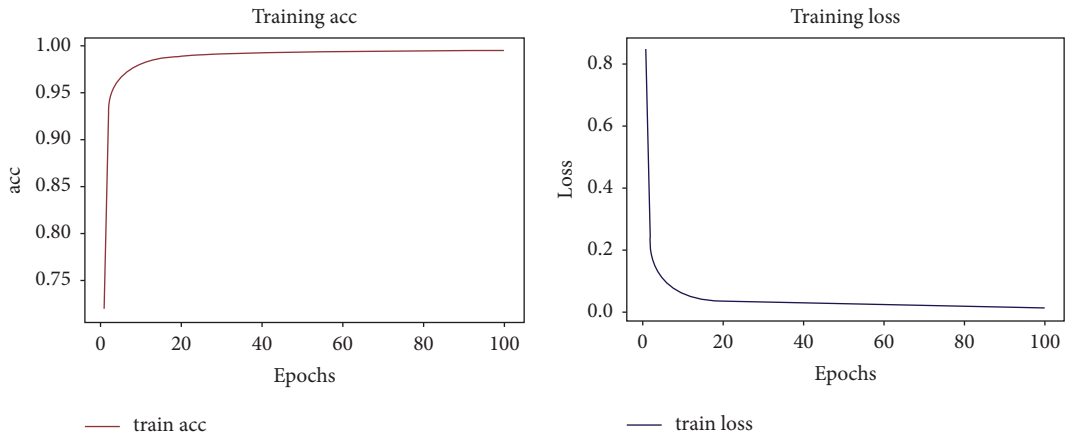

Figure 13: The training acc and loss of the CNN model.

Table 6: Parameter of the external excitation in these cases.

Category	Range of taking value
Reduction coefficient α_i	Random numbers evenly distributed between 0.3 and 1.0
Magnitude of pulse excitation	30 N~100 N uniformly distributed random number
Direction of pulse excitation	Vertical down
Action position of pulse excitation	Random number of 2~20 nodes uniformly distributed

5×100 Matrix

Measurement points 1	$x1, 1$	$x1, 2$	···	$x1, i$	$x1, j$	···	$x1, 98$	$x1, 99$	$x1, 100$
Measurement points 2	$x2, 1$	$x2, 2$	···	$x2, i$	$x2, j$	···	$x2, 98$	$x2, 99$	$x2, 100$
Measurement points 3	$x3, 1$	$x3, 2$	···	$x3, i$	$x3, j$	···	$x3, 98$	$x3, 99$	$x3, 100$
Measurement points 4	$x4, 1$	$x4, 2$	···	$x4, i$	$x4, j$	···	$x4, 98$	$x4, 99$	$x4, 100$
Measurement points 5	$x5, 1$	$x5, 2$	···	$x5, i$	$x5, j$	···	$x5, 98$	$x5, 99$	$x5, 100$

Figure 14: CNN's input data.

Table 7: Mean value and COV of structural parameters.

Structural parameters	Mass density (kg/m^3)	Modulus of elasticity (MPa)	Damping ratio
Mean value μ	2500	3.0×10^4	0.02
COV δ	Both 0, 0.05, 0.10, 0.15, 0.20, 0.25 and 0.30		

$$\mathrm{SNR} = \frac{\text{signal energy}}{\text{noise energy}} = \frac{\text{pure signal}^2}{(\text{noisy signal} - \text{pure signal})^2}. \quad (2)$$

Based on two types of the established CNN model considering various COVs for uncertainties, three cases with different SNR, such as SNR = 10, 5, and 1, are simulated to investigate the applicability of SDI by CNN, and the results are shown in Figure 20. It is significantly noted that the effects of the SNR on the IR for the CNN 1 model are much bigger than those for the CNN 2 model. The differences in IR calculated by two CNN models are increasing with the development of the COVs of uncertainties and the noise involved in measuring information. When the COVs of uncertainties is 0.1, the differences in IR by two CNN models can reach 10% for SNR = 1. However, those differences can nearly be 1% without any noise. Therefore, due to the unavoidable noises arising from the measurement, the uncertain parameters should be considered in the training data for the CNN model, and the accuracy of the structural damage situation identified by CNN is more essential with more noises involved in the measurement.

5. Effect of Nonuniform Measuring Condition on the SDI Based on CNN

For the actual operating SDI environment, the sensors must face the situation of unavoidable measuring noise and damage, which induce the nonuniform characteristics of measurement for the SDI. During the collecting signals process of SDI, there should be measuring noises with irregularity and varying intensities. Most of these are additive noise, which is independent of the available signals. Similar to Image Recognition, when the eyes deal with the significant signals from the image, the noise will affect the uniformity of the key information in the signals. As shown in Figure 21, the letter "A" in the picture is required information, and the background of the picture means noise. The noise is uniformly filled in the background, and the intensity of the noise is increasing with the darker background. The effect of the intensities of uniform noise on image recognition is significant.

However, if the effect of noise on every measuring channel is the same, uniform characteristics are exhibited. In contrast to this, the intensities of noises are different, which will present the spatial nonuniform characteristics of measurement. As shown in Figure 22, the background has been divided into 25 subspaces, and the varying intensities of noise affect the random independent subspaces. For the SDI based on CNN, it is necessary to investigate the effect of nonuniform noises on the accuracy of recognition.

Meanwhile, multisensor damage is an extreme situation for the nonuniform condition in measurement. As shown in Figure 23, there are 5 sensors to collect information, and the accuracy of every sensor is independent and random. When a certain sensor is damaged, the measured signal is defined as noise. It is also significant to study the effect of the multisensor damaged situation on the accuracy of the CNN for the SDI.

To increase the computational efficiency of the CNN in nonuniform measuring conditions, the Latin hypercube sampling (LHS) is applied to deal with the randomness of the noise. The cases of noise are listed in Table 11.

As listed in the table, SNR (15, 1) shows that the mean value of noise is 15 based on the signal-to-noise ratio, and the variance is 1 which reflects the nonuniformity. To investigate the effect of the nonuniform noise on CNNs, the mean value stays constant and the variance varies in all the cases.

Taking Issue 1 as an example to show the application of LHS, the prepared condition is listed in Table 12. There are 5 channels in this testing, so the number of random variable (n) is defined as 5 and the sampling time (N) is 10. A random integer arrangement r_i^j of 1~10 is generated based on every random variable X_i, and r_i^j will be rearranged from small to big. The rearranged samples are selected to build the CNN framework, and the samples of three cases are listed in Tables 12–15.

The simulated nonuniform acceleration responses are selected as the prediction samples which are used to identify structural damage based on CNNs. As a result, the nonuniform conditions in measurement have a significant influence on the identified accuracy by CNNs. The mean value of identified results is decreasing with the development of the variance of nonuniform noise, but the variance of that is increasing. The biggest variance of the noise, which belongs to Issue 3, leads to the smallest mean value and biggest variance of the results identified by CNN. In addition, Issue 1 has the smallest variance of identified results, which means the distributing range of the identified result is the smallest and the most stable of results is exhibited. The stability of identified results is increasing with the development of nonuniform characteristics of noise. Therefore, the mean value of identified results reflects the accuracy of SDI based on CNNs, and variance shows the stability of identification. If the measuring noises present more obvious nonuniform characteristics, the accuracy and stability of SDI based on CNNs will deteriorate.

Several sensors settle on the structure, which are applied to capture dynamic responses, and structural health monitoring systems contain different types of sensors with different capturing accuracy. Missing data will cause

Table 8: The details of the involved cases.

Case of text	Description of case of text	
	Training network	Prediction network
1	The randomness of structural parameters is not considered	Only the randomness of mass is considered
2	The randomness of structural parameters is not considered	Only the randomness of elastic modulus is considered
3	The randomness of structural parameters is not considered	Only the randomness of damping ratio is considered
4	The randomness of structural parameters is not considered	Considering the randomness of mass, elastic modulus and damping ratio working together

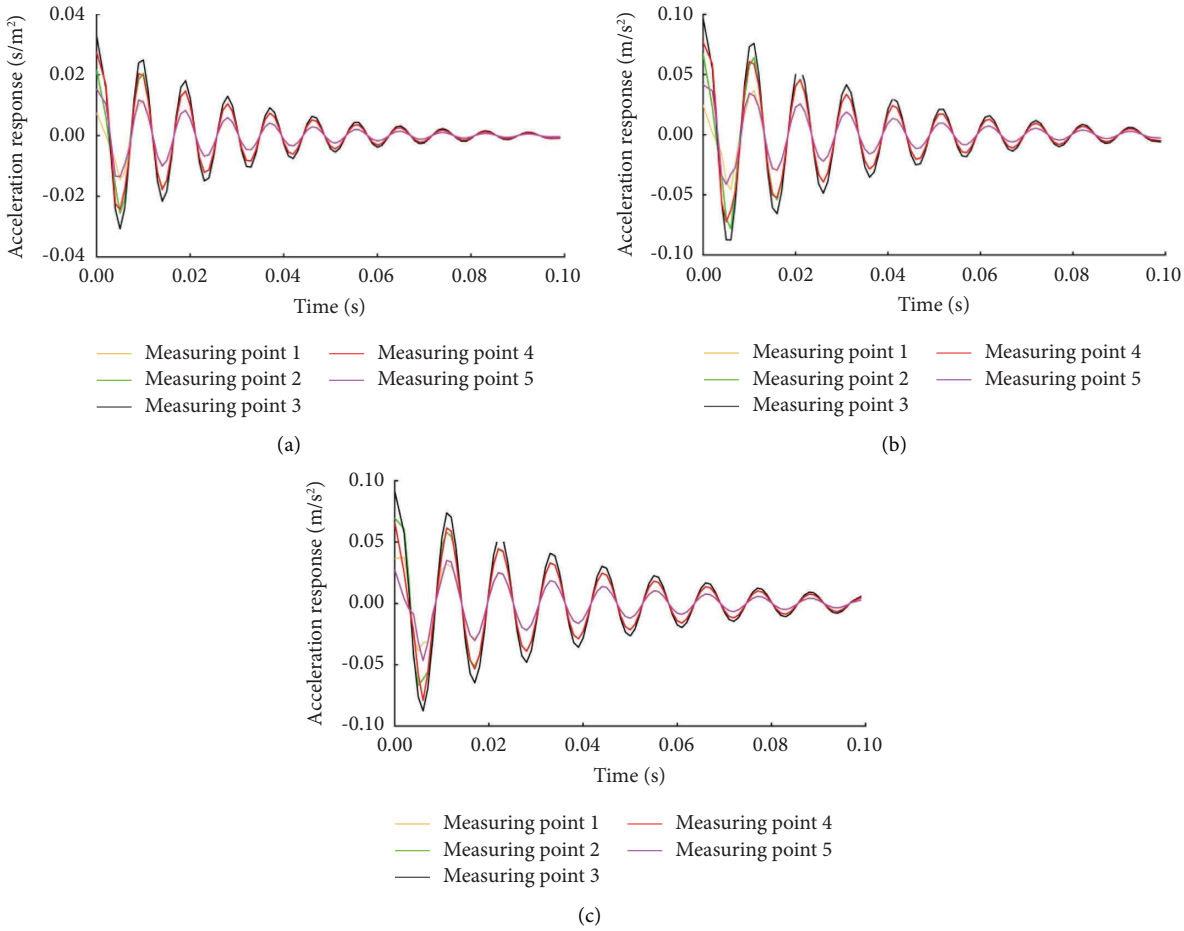

Figure 15: Acceleration response of structure under a pulse excitation in case 1 (a) when COV is 0.1; (b) when COV is 0.2; (c) when COV is 0.3.

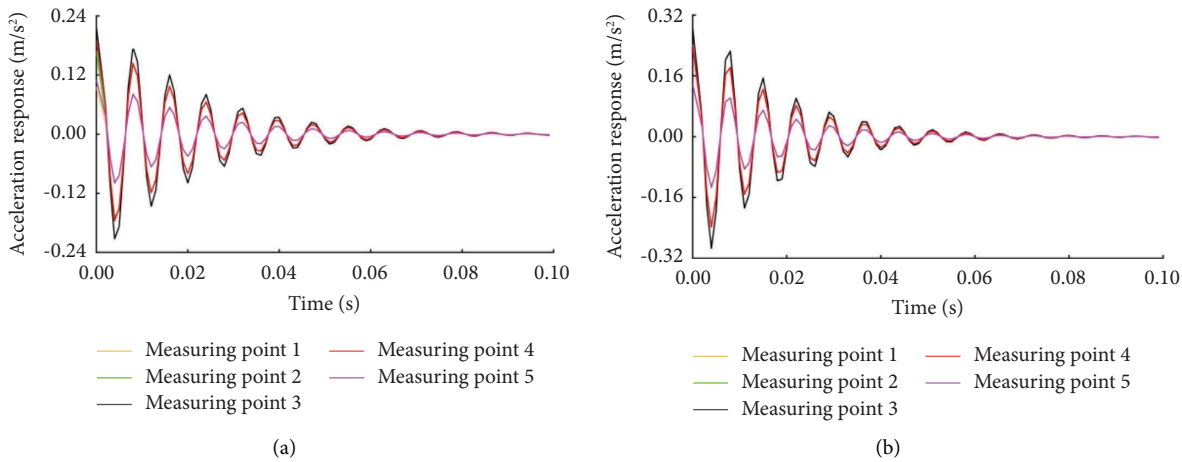

Figure 16: Continued.

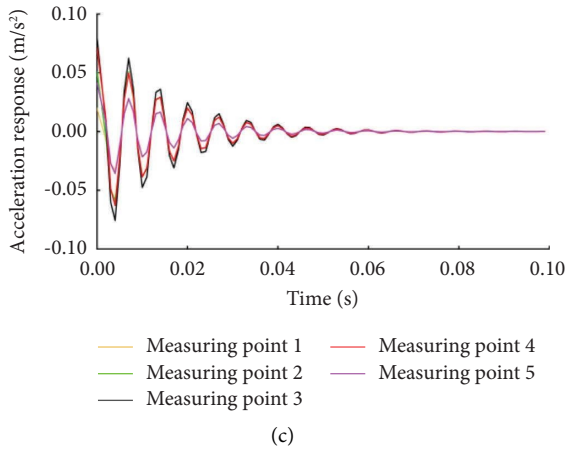

Figure 16: Acceleration response of the structure under a pulse excitation in case 2 (a) when COV is 0.1; (b) when COV is 0.2; (c) when COV is 0.3.

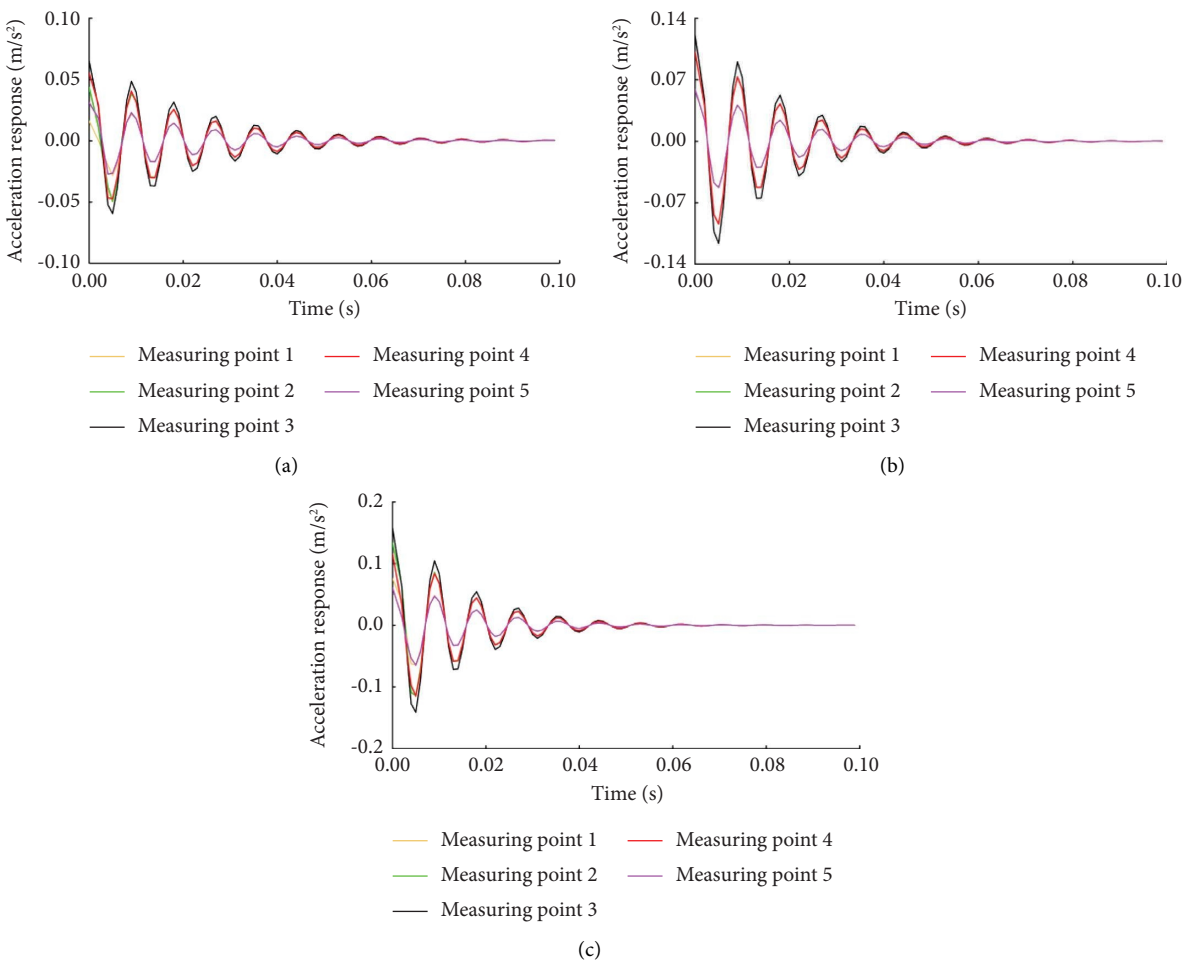

Figure 17: Acceleration response of the structure under a pulse excitation in case 3 (a) when COV is 0.1; (b) when COV is 0.2; (c) when COV is 0.3.

significant information to get lost and decrease the reliability of SDI, and it is an extreme situation for the nonuniform condition in measurement. Therefore, it is essential to investigate the effect of missing data on the SDI based on CNN. Based on the simply supported bridge, the multisensor damage state is simulated in experimental testing, and the details of the cases are exhibited in Figure 8. As an assumption, a working sensor can capture the

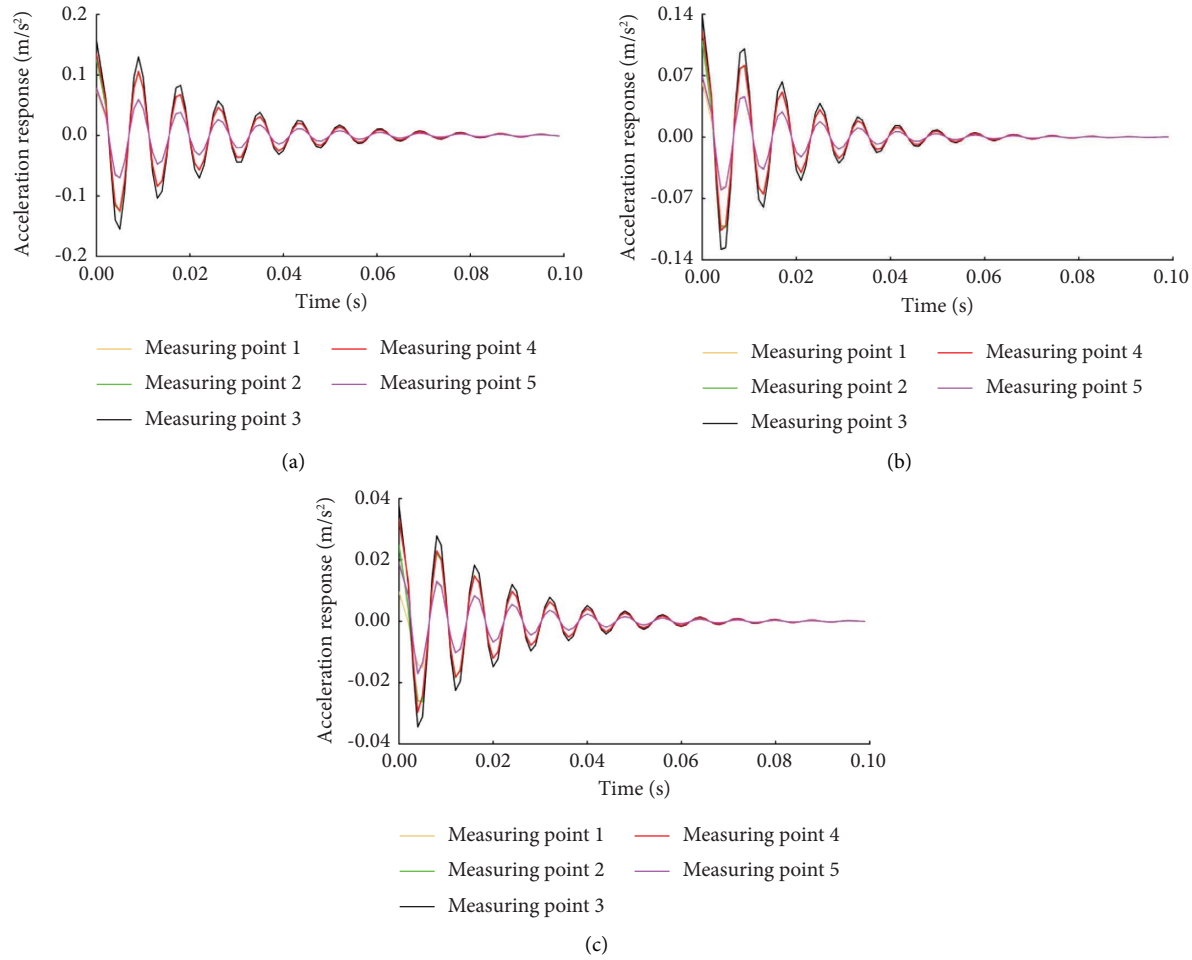

FIGURE 18: Acceleration response of the structure under a pulse excitation in case 4 (a) when COV is 0.1; (b) when COV is 0.2; (c) when COV is 0.3.

responses without noise, and a damaged sensor just gets noise. The acceleration responses conducted by sensors in tests are listed in Figures 24 and 25.

The results conducted by the FE model and experimental testing are, respectively, selected as training data for the CNN model, and the IR of the SDI based on CNN is shown in Figure 26. When one sensor is damaged, the nonuniform characteristics are not strong. However, the corresponding IRs stay in a range of 60~78% for Case 2~4 which nearly cannot satisfy the requirement of the SDI. In addition, as the damaged sensors settle closer to the midspan of the bridge, the IR gets smaller. With 2-3 damaged sensors, the accuracies of the SDI based on CNN are further decreasing, and their IRs are just bigger than 50%, which cannot be adopted in the engineering application. If only one sensor is working, the IR is smaller than 40%. Therefore, the multisensor damaged condition, which is the extreme issue of the nonuniform condition in measurement, has a significant influence on the SDI based on CNN.

The accuracy of SDI is rapidly decreasing with the development of nonuniform characteristics presented in the capturing signals.

Table 9: CNN's parameters of the uncertain structure.

Network layer	Module	Input points	Computing cores	Computing cores	Sliding step	Output points
L1	Input layer	$1@5\times100$	—	—	—	$1@5\times100$
L2	Convolutional layer C1	$1@5\times100$	5	3×3	1	$5@5\times100$
L3	Pooling layer P1	$5@5\times100$	1	2×2	2	$5@3\times50$
L4	Convolutional layer C2	$5@3\times50$	5	3×3	1	$5@3\times50$
L5	Pooling layer P2	$5@3\times50$	1	2×2	2	$5@2\times25$
L6	Convolutional layer C3	$5@2\times25$	5	3×3	1	$5@2\times25$
L7	Pooling layer P3	$5@2\times25$	1	2×2	2	$5@1\times13$
L8	Fully connected layer F1	$5@1\times13$	—	—	—	$1@1\times65$
L9	Fully connected layer F2	$1@1\times65$	—	—	—	$1@1\times40$
L10	Fully connected layer F3	$1@1\times40$	—	—	—	$1@1\times10$
L11	Softmax layer	$1@1\times10$	—	—	—	$1@1\times2$
L12	Output layer	$1@1\times2$	—	—	—	The probability of two categories of "0" and "1"

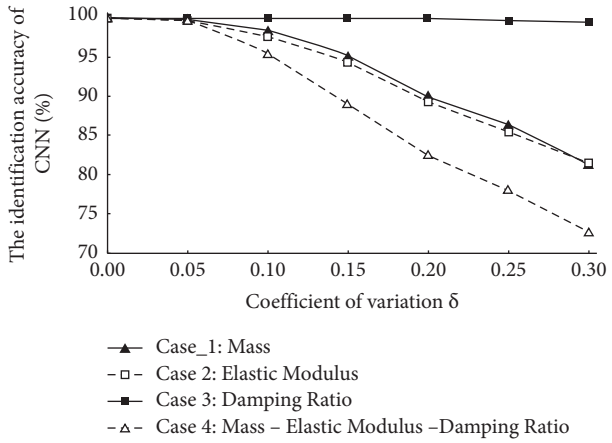

Figure 19: CNN identification accuracy of the uncertain structure.

Table 10: Identification accuracy of two network models without noise influence.

COV (%)	0.00	0.05	0.10	0.15	0.20	0.25	0.30
Network model 1	99.95	99.60	95.25	88.90	82.43	77.93	72.55
Network model 2	99.98	99.95	97.25	90.53	83.83	78.20	72.68
Difference 2-1	0.03	0.04	2.00	1.63	1.40	0.27	0.13

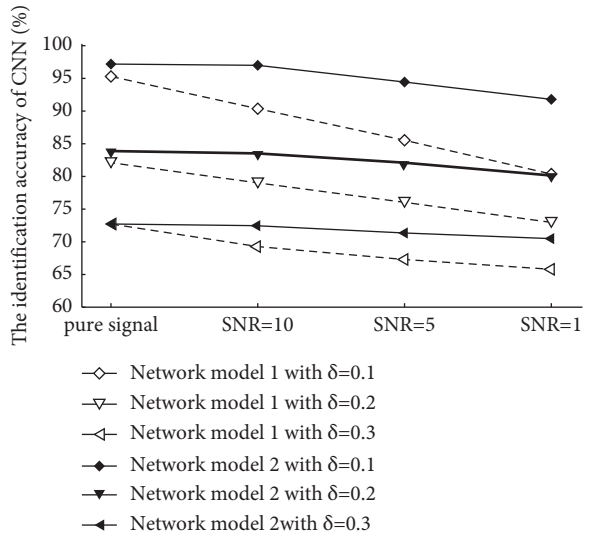

Figure 20: Identification accuracy between network model 1 and 2 under different SNRs.

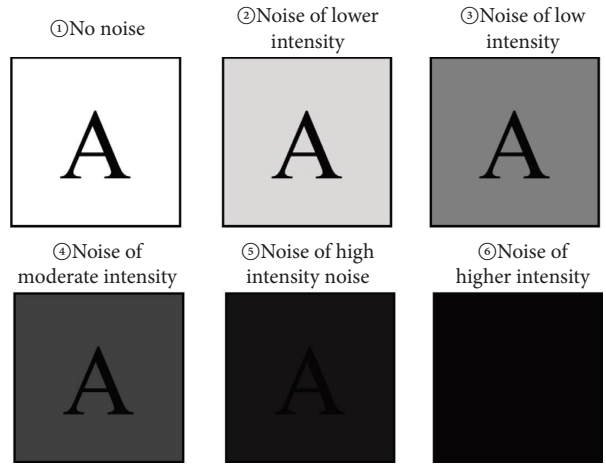

Figure 21: Effect of uniform noise on recognized information.

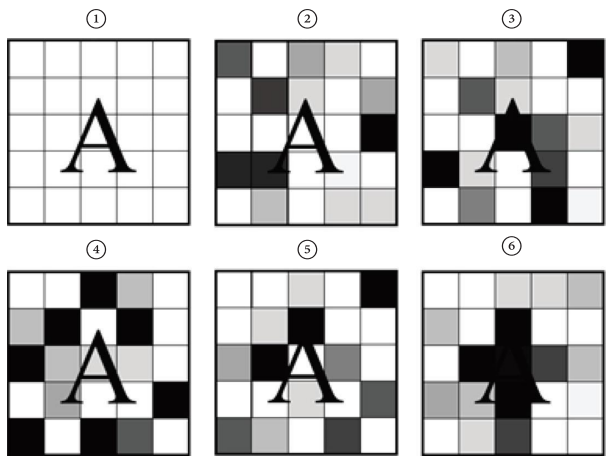

Figure 22: Effect of nonuniform noise on recognized information.

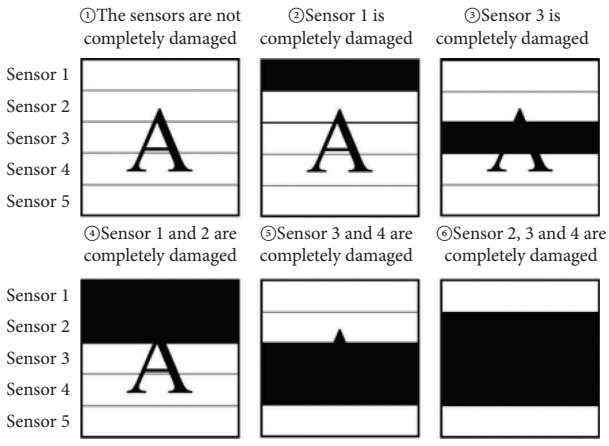

Figure 23: Multisensors damaged condition in the measurement.

Table 11: Case of adding noise.

Serial number	Normal distribution of noise (mean, variance) $N(\mu, \sigma)$
Issue 1	N (15, 1.0)
Issue 2	N (15, 2.5)
Issue 3	N (15, 5.0)

Table 12: Calculation process of LHS with Issue 1.

N	PDF	P_j	$X_i^j = f(P_j, \mu, \sigma)$	r_1^j	r_2^j	r_3^j	r_4^j	r_5^j
1	0.0~0.1	0.05	$X_i^1 = (0.05, 15, 1) = 13.3551$	1	9	4	7	7
2	0.1~0.2	0.15	$X_i^2 = (0.15, 15, 1) = 13.9636$	6	6	8	6	8
3	0.2~0.3	0.25	$X_i^3 = (0.25, 15, 1) = 14.3255$	7	5	9	1	4
4	0.3~0.4	0.35	$X_i^4 = (0.35, 15, 1) = 14.6147$	5	2	5	10	3
5	0.4~0.5	0.45	$X_i^5 = (0.45, 15, 1) = 14.8743$	9	10	6	9	9
6	0.5~0.6	0.55	$X_i^6 = (0.55, 15, 1) = 15.1257$	4	8	1	4	2
7	0.6~0.7	0.65	$X_i^7 = (0.65, 15, 1) = 15.3853$	10	4	2	2	5
8	0.7~0.8	0.75	$X_i^8 = (0.75, 15, 1) = 15.6745$	8	3	7	5	10
9	0.8~0.9	0.85	$X_i^9 = (0.85, 15, 1) = 16.0364$	3	7	3	3	1
10	0.9~1.0	0.95	$X_i^{10} = (0.95, 15, 1) = 16.6449$	2	1	10	8	6

Table 13: Value of LHS with Issue 1.

Sample number	SNR in channel 1	SNR in channel 2	SNR in channel 3	SNR in channel 4	SNR in channel 5
Sample 1-1	13.3551	16.6449	15.1257	14.3255	16.0364
Sample 1-2	16.6449	14.6147	15.3853	15.3853	15.1257
Sample 1-3	16.0364	15.6745	16.0364	16.0364	14.6147
Sample 1-4	15.1257	15.3853	13.3551	15.1257	14.3255
Sample 1-5	14.6147	14.3255	14.6147	15.6745	15.3853
Sample 1-6	13.9636	13.9636	14.8743	13.9636	16.6449
Sample 1-7	14.3255	16.0364	15.6745	13.3551	13.3551
Sample 1-8	15.6745	15.1257	13.9636	16.6449	13.9636
Sample 1-9	14.8743	13.3551	14.3255	14.8743	14.8743
Sample 1-10	15.3853	14.8743	16.6449	14.6147	15.6745

Table 14: Value of LHS with Issue 2.

Sample number	SNR in channel 1	SNR in channel 2	SNR in channel 3	SNR in channel 4	SNR in channel 5
Sample 2-1	13.3138	10.8879	15.3142	13.3138	15.3142
Sample 2-2	12.4089	19.1121	12.4089	19.1121	19.1121
Sample 2-3	15.9633	14.0367	14.0367	10.8879	14.0367
Sample 2-4	17.5911	14.6858	17.5911	15.3142	14.6858
Sample 2-5	19.1121	12.4089	13.3138	16.6862	13.3138
Sample 2-6	14.0367	15.3142	16.6862	17.5911	10.8879
Sample 2-7	16.6862	13.3138	15.9633	12.4089	17.5911
Sample 2-8	15.3142	15.9633	19.1121	14.6858	16.6862
Sample 2-9	10.8879	16.6862	10.8879	14.0367	15.9633
Sample 2-10	14.6858	17.5911	14.6858	15.9633	12.4089

Table 15: Value of LHS with noise Issue 3.

Sample number	SNR in channel 1	SNR in channel 2	SNR in channel 3	SNR in channel 4	SNR in channel 5
Sample 3-1	15.6283	9.8178	14.3717	18.3724	11.6276
Sample 3-2	16.9266	23.2243	6.7757	6.7757	9.8178
Sample 3-3	9.8178	18.3724	20.1822	14.3717	20.1822
Sample 3-4	18.3724	13.0734	23.2243	11.6276	23.2243
Sample 3-5	14.3717	15.6283	15.6283	13.0734	6.7757
Sample 3-6	6.7757	6.7757	18.3724	20.1822	14.3717
Sample 3-7	11.6276	11.6276	16.9266	16.9266	13.0734
Sample 3-8	13.0734	16.9266	11.6276	15.6283	15.6283
Sample 3-9	20.1822	14.3717	13.0734	23.2243	16.9266
Sample 3-10	23.2243	20.1822	9.8178	9.8178	18.3724

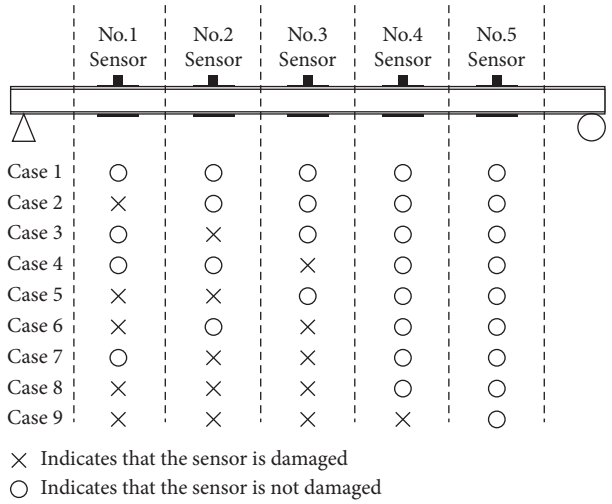

Figure 24: Schematic of sensor to simulate nonuniform.

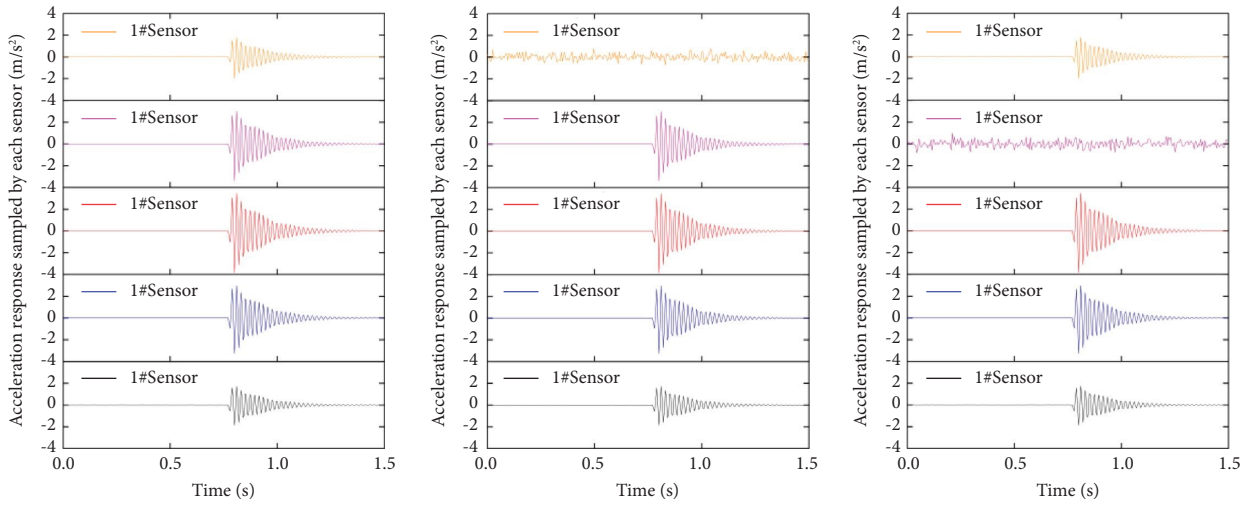

Figure 25: Continued.

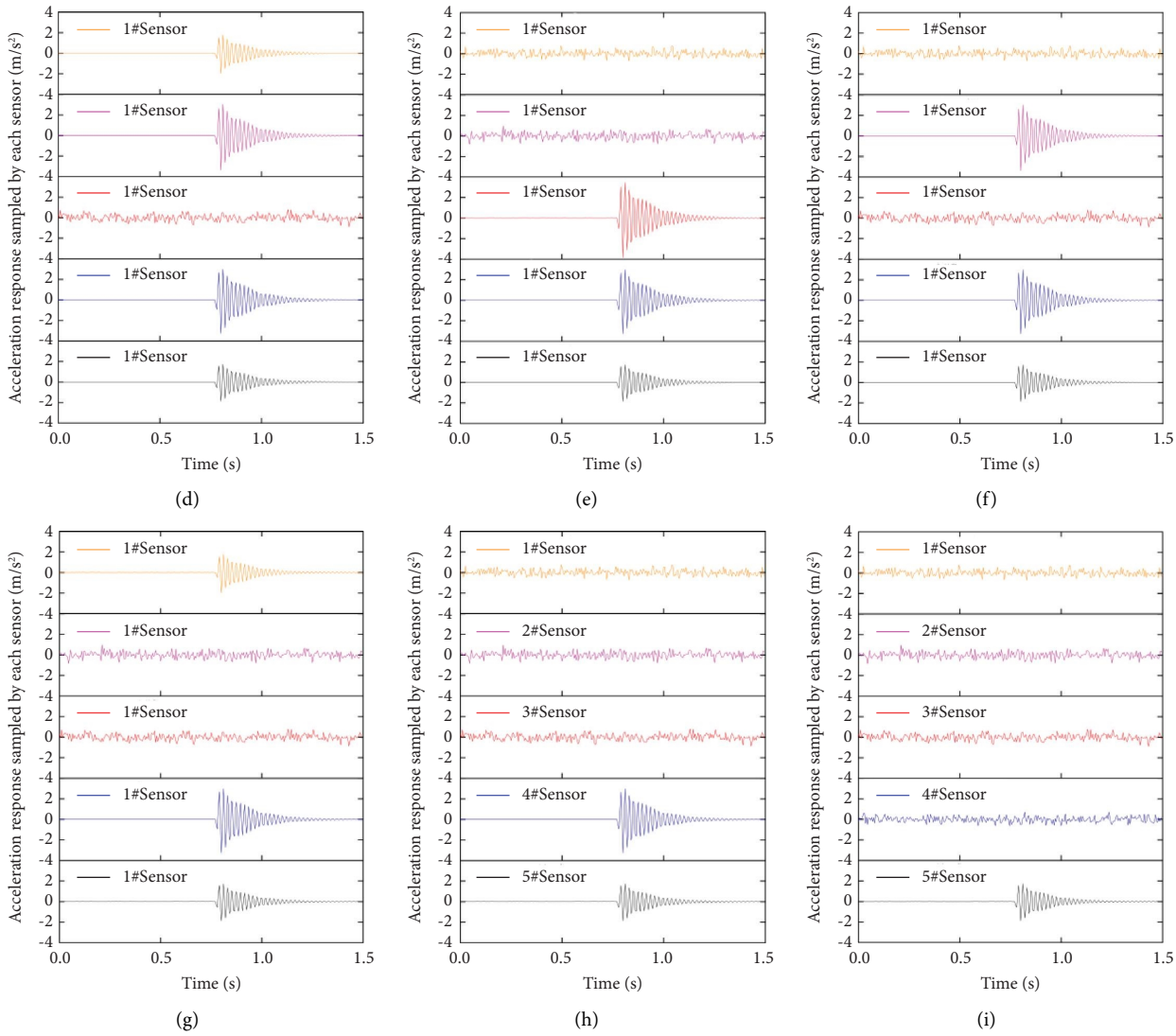

Figure 25: Acceleration response signals collected by sensors under various cases. (a) Case 1. (b) Case 2. (c) Case 3. (d) Case 4. (e) Case 5. (f) Case 6. (g) Case 7. (h) Case 8. (i) Case 9.

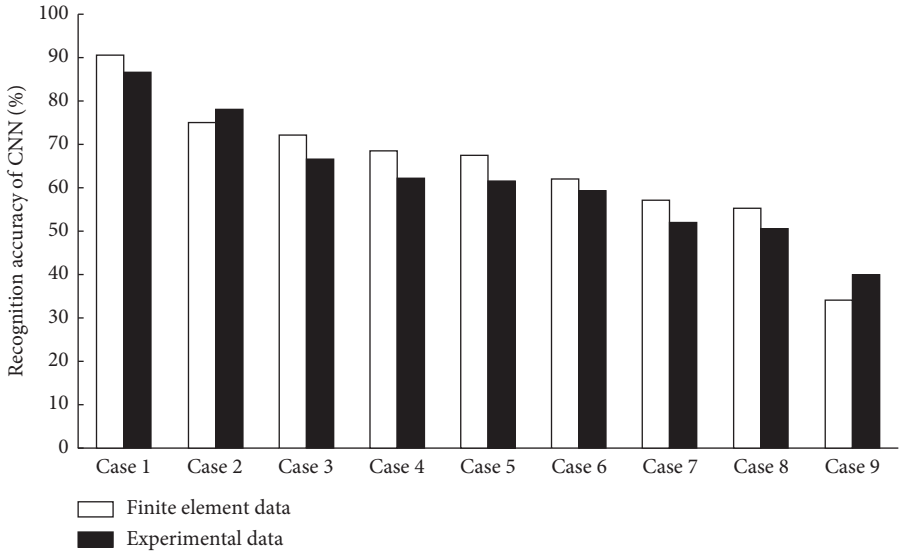

Figure 26: Comparison of CNN identification accuracy under different cases.

6. Conclusion

This study proposes a novel CNN architecture for SDI and investigates the accuracy and effectiveness by finite element analysis and experimental testing. The effects of the unavoidable uncertainties and nonuniform characteristics in measurement condition on the identification accuracy of the CNNs for SDI are studied. The main details of the conclusion are listed as follows.

(1) The proposed architecture of CNN for SDI consists of 12 layers, including 1 input layer, 3 convolution layers, 3 pooling layers, 3 full connection layers, 1 Softmax layer, and 1 output layer, whose identification accuracy is verified by comparison with the numerical and experimental data.

(2) The structure uncertainties have a significant influence on the identification accuracy of the CNN, and the IRs are decreasing with the increasing COV of elastic modulus and mass. If the captured signals by sensors consider the measuring noise, the training data for the CNN should also adopt the acceleration responses with structural uncertainties.

(3) The strong nonuniform characteristics in measurement condition make the identification accuracy of CNN for SDI not satisfy the computational requirement, especially for the multisensors damaged states. Therefore, the data imputation method should be studied to handle the missing data situation in the future work.

Data Availability

The data used in this study are available on request from the author.

Conflicts of Interest

The authors declare that they have no conflicts of interest.

Acknowledgments

The authors are grateful for the financial support from the National Natural Science Foundation of China (Grant nos. 52178453 and 51908076), Key Research and Development Program by Science and Technology Department of Sichuan Province (Grant no. 22ZDYF3059), and China Postdoctoral Science Foundation (Grant nos. 2020M673155 and 2022T150755).

References

[1] S. W. Doebling, C. R. Farrar, M. B. Prime, and M., B. Prime, "A summary review of vibration-based damage identification methods," *The Shock and Vibration Digest*, vol. 30, no. 2, pp. 91–105, 1998.

[2] R. R. Hou and Y. Xia, "Review on the new development of vibration-based damage identification for civil engineering structures: 2010–2019," *Journal of Sound Vibration*, vol. 491, Article ID 115741, 2021.

[3] L. Grassia, M. Iannone, A. Califano, and A. D'Amore, "Strain based method for monitoring the health state of composite structures," *Composites Part B: Engineering*, vol. 176, Article ID 107253, 2019.

[4] Z. Tang, Z. Chen, Y. Bao, and H. Li, "Convolutional neural network-based data anomaly detection method using multiple information for structural health monitoring," *Structural Control and Health Monitoring*, vol. 26, no. 1, Article ID e2296, 2019.

[5] X. W. Ye, J. Tao, and C. B. Yun, "A review on deep learning-based structural health monitoring of civil infrastructures," *Smart Structures and Systems*, vol. 24, pp. 567–585, 2019.

[6] O. Abdeljaber, O. Avci, S. Kiranyaz, M. Gabbouj, and D. J. Inman, "Real-time vibration-based structural damage detection using one-dimensional convolutional neural networks," *Journal of Sound and Vibration*, vol. 388, pp. 154–170, 2017.

[7] Y. Duan, C. Qianyi, H. Zhang, C. Yun, S. Wu, and Q. Zhu, "CNN-based damage identification method of tied-arch bridge using spatial-spectral information," *Smart Structures and Systems*, vol. 23, pp. 507–520, 2019.

[8] Y. Bao, Z. Tang, H. Li, and Y. Zhang, "Computer vision and deep learning-based data anomaly detection method for structural health monitoring," *Structural Health Monitoring*, vol. 18, no. 2, pp. 401–421, 2019.

[9] R. Wang, J. Li, S. Chencho et al., "Densely connected convolutional networks for vibration based structural damage identification," *Engineering Structures*, vol. 245, Article ID 112871, 2021.

[10] Y. Xu, Y. Bao, J. Chen, W. Zuo, and H. Li, "Surface fatigue crack identification in steel box girder of bridges by a deep fusion convolutional neural network based on consumer-grade camera images," *Structural Health Monitoring*, vol. 18, no. 3, pp. 653–674, 2018.

[11] P. Seventekidis, D. Giagopoulos, A. Arailopoulos, and O. Markogiannaki, "Structural Health Monitoring using deep learning with optimal finite element model generated data," *Mechanical Systems and Signal Processing*, vol. 145, Article ID 106972, 2020.

[12] M. Li, D. Jia, Z. Wu, S. Qiu, and W. He, "Structural damage identification using strain mode differences by the iFEM based on the convolutional neural network (CNN)," *Mechanical Systems and Signal Processing*, vol. 165, Article ID 108289, 2022.

[13] T. Zhang, D. Shi, Z. Wang, P. Zhang, S. Wang, and X. Ding, "Vibration-based structural damage detection via phase-based motion estimation using convolutional neural networks," *Mechanical Systems and Signal Processing*, vol. 178, Article ID 109320, 2022.

[14] D. Ai, F. Mo, Y. Han, and J. Wen, "Automated identification of compressive stress and damage in concrete specimen using convolutional neural network learned electromechanical admittance," *Engineering Structures*, vol. 259, Article ID 114176, 2022.

[15] R. Falcone, C. Lima, and E. Martinelli, "Soft computing techniques in structural and earthquake engineering: a literature review," *Engineering Structures*, vol. 207, Article ID 110269, 2020.

[16] A. Kaveh and A. Dadras, "Structural damage identification using an enhanced thermal exchange optimization

algorithm," *Engineering Optimization*, vol. 50, no. 3, pp. 430–451, 2018.

[17] S. Khatir, M. Abdel Wahab, D. Boutchicha, and T. Khatir, "Structural health monitoring using modal strain energy damage indicator coupled with teaching-learning-based optimization algorithm and isogoemetric analysis," *Journal of Sound and Vibration*, vol. 448, pp. 230–246, 2019.

[18] E. Sevillano, R. Sun, and R. Perera, "Damage evaluation of structures with uncertain parameters via interval analysis and FE model updating methods," *Structural Control and Health Monitoring*, vol. 24, no. 4, Article ID e1901, 2017.

[19] C. Soize, "Stochastic modeling of uncertainties in computational structural dynamics—recent theoretical advances," *Journal of Sound and Vibration*, vol. 332, no. 10, pp. 2379–2395, 2013.

[20] C. S. N. Pathirage, J. Li, L. Li, H. Hao, W. Liu, and P. Ni, "Structural damage identification based on autoencoder neural networks and deep learning," *Engineering Structures*, vol. 172, pp. 13–28, 2018.

[21] L. G. G. Villani, S. da Silva, and A. Cunha, "Damage detection in uncertain nonlinear systems based on stochastic Volterra series," *Mechanical Systems and Signal Processing*, vol. 125, pp. 288–310, 2019.

[22] L. G. G. Villani, S. Silva, and A. Cunha, "Damage detection in an uncertain nonlinear beam," *Procedia Engineering*, vol. 199, pp. 2090–2095, 2017.

[23] Z. Ding, J. Li, H. Hao, and Z.-R. Lu, "Structural damage identification with uncertain modelling error and measurement noise by clustering based tree seeds algorithm," *Engineering Structures*, vol. 185, pp. 301–314, 2019.

[24] G. Fan, J. Li, and H. Hao, "Vibration signal denoising for structural health monitoring by residual convolutional neural networks," *Measurement*, vol. 157, Article ID 107651, 2020.

[25] Q. Shi, K. Hu, L. Wang, and X. Wang, "Uncertain identification method of structural damage for beam-like structures based on strain modes with noises," *Applied Mathematics and Computation*, vol. 390, Article ID 125682, 2021.

[26] G. L. S. Silva, D. A. Castello, L. Borges, and J. P. Kaipio, "Damage identification in plates under uncertain boundary conditions," *Mechanical Systems and Signal Processing*, vol. 144, Article ID 106884, 2020.

[27] G. L. S. Silva, D. A. Castello, and J. P. Kaipio, "Damage identification under uncertain mass density distributions," *Computer Methods in Applied Mechanics and Engineering*, vol. 376, Article ID 113672, 2021.

[28] Y. Bao and H. Li, "Machine learning paradigm for structural health monitoring," *Structural Health Monitoring*, vol. 20, no. 4, pp. 1353–1372, 2020.

[29] R. Wang, S. Chencho, S. An et al., "Deep residual network framework for structural health monitoring," *Structural Health Monitoring*, vol. 20, no. 4, pp. 1443–1461, 2020.

[30] Y. Zhang, Y. Miyamori, S. Mikami, and T. Saito, "Vibration-based structural state identification by a 1-dimensional convolutional neural network," *Computer-Aided Civil and Infrastructure Engineering*, vol. 34, no. 9, pp. 822–839, 2019.

[31] Y. Bao, Z. Chen, S. Wei, Y. Xu, Z. Tang, and H. Li, "The state of the art of data science and engineering in structural health monitoring," *Engineering*, vol. 5, no. 2, pp. 234–242, 2019.

[32] J. Hou, H. Jiang, C. Wan et al., "Deep learning and data augmentation based data imputation for structural health monitoring system in multi-sensor damaged state," *Measurement*, vol. 196, Article ID 111206, 2022.

[33] G. Fan, J. Li, and H. Hao, "Lost data recovery for structural health monitoring based on convolutional neural networks," *Structural Control and Health Monitoring*, vol. 26, no. 10, Article ID e2433, 2019.

[34] G. Fan, J. Li, and H. Hao, "Dynamic response reconstruction for structural health monitoring using densely connected convolutional networks," *Structural Health Monitoring*, vol. 20, no. 4, pp. 1373–1391, 2020.

[35] X. Lei, L. Sun, Y. Xia, L. Sun, and Y. Xia, "Lost data reconstruction for structural health monitoring using deep convolutional generative adversarial networks," *Structural Health Monitoring*, vol. 20, no. 4, pp. 2069–2087, 2021.

[36] K. Yang, W. Tong, Z. Huang, T. Qiu, and Z. Lai, "Signal-to-noise ratio improvement of the signal immersed in the strong background noise using a bistable circuit with tunable potential-well depth," *Mechanical Systems and Signal Processing*, vol. 177, Article ID 109201, 2022.